Modeling of pH-Switchable Ion Transport and Selectivity in Nanopore Membranes with Fixed Charges

Patricio Ramírez,*,† Salvador Mafé,‡ Antonio Alcaraz,§ and Javier Cervera‡

Departamento de Física Aplicada, Universidad Politécnica de Valencia, E-46022 Valencia, Spain, Departament de Termodinàmica, Universitat de Valencia, E-46100 Burjassot, Spain, and Departament de Ciencies Experimentals, Universitat Jaume I, E-12080 Castelló, Spain

Received: June 23, 2003

The pH-switchable ion transport and selectivity in nanopore membranes with fixed charges is theoretically analyzed using a model based on the Nernst−Planck flux equations. The ionization state of the weak polyelectrolyte groups attached to the pore surface appears to be a crucial factor in order to understand the conductive properties of the pore. The model allows for the calculation of the fluxes of all of the ionic species involved and the membrane potential. Comparison of the theoretical results with the experimental data by Martin el al. (*Science* **1995**, *268*, 700−2; *J. Phys. Chem. B* **2001**, *105*, 1925−34; and *Adv. Mater.* **2001**, *13*, 1351−62) and Stroeve et al. (*Langmuir* **2000**, *16*, 2401−4; and *Langmuir* **2001**, *17*, 5271−5) for surface modified nanopores with fixed charges shows that the model can describe qualitatively the changes of the permeate ion flux and the membrane potential with the pH and the solute concentration of the external solutions. The effect of applying an electric potential to the nanopore walls is also studied. Some of the main characteristics that allow a simple description of pH-switchable effects on nanopore membranes with fixed charges are clearly shown.

I. Introduction

Transport phenomena in many biophysical systems and biotechnological applications involve the permeation of ionic species through fixed charge membranes.[1−10] Because the local pH and electrolyte concentration of the membrane solution regulates the ionization state of the membrane fixed charges[5,7] and the permeate ion,[4,8] the transport rates can be adjusted by the external solutions. It has been shown[5−7] that the permeability to an ionic drug of a fixed charge membrane changes by several orders of magnitude when the external pH is varied. Also, pH effects are important in thick biological membranes such as the human skin[9] and the cornea,[10] where differences in the permeabilities between cationic and anionic species have been ascribed to the existence of fixed charges within the membrane. Recent experimental studies by Martin el al[11−14] and Stroeve et al.[15,16] have shown the remarkable electrochemical characteristics of pH-switchable membranes with fixed charges attached to the inside nanopore walls. In both cases, the modification of the pore surface permits membranes with unique ion transport and selectivity properties to be obtained. Pores of molecular dimensions and high ionic selectivity are characteristic of ionic channels in biomembranes,[1,17] and therefore, synthetic membranes with surface modified narrow pores can also be used to mimic the behavior of biological membranes.[18−24]

We study here if extensions of a continuous model capable of describing the ionic transport and selectivity of fixed charge membranes with wide pores[1,7,8,25−29] could be useful for nanopore membranes (see ref 30 for the case of ionic channels). To this end, we analyze theoretically recent experimental results by Martin et al.[14,31,32] and Stroeve et al.[15,16] corresponding to surface modified nanopores with fixed charges. These studies cover a broad range of membranes and membrane characteristics (permeate fluxes and membrane potential) under different experimental conditions (pH, membrane fixed charge and permeate concentrations, and electric potential applied to the nanopore surfaces). The theoretical approach employed is based on the Nernst−Planck flux equations[1,33] with the Goldman constant field assumption,[34] and all ionic species present in the system (the permeate and salt ions together with the hydrogen and hydroxide) are taken into account. In all cases, the ionization state of the weak polyelectrolyte groups on the pore surface is obtained using of the local pH within the membrane.[35−37]

The results presented can be relevant for the analysis of the pH dependent transport of an ionic permeate through thick membranes containing narrow pores. Experiments with these systems are often conducted using a buffer solution, and the measured multiionic system properties are analyzed in terms of simple binary salt system equations. Moreover, the internal pH within the membrane is often assumed to be approximately equal to the pH of the external solution. These assumptions can introduce severe errors[8,38] in the analysis of experimental data and will not be used here. The comparison of the theoretical results with experiments show that the model explains qualitatively the changes of the permeate flux and the membrane potential with the pH, the solute concentration of the external solution, and the electric potential applied to the nanopore walls.

II. Theory

Figure 1a shows a schematic view of the membrane that consists of a porous polymeric support with a gold layer

* To whom correspondence should be addressed. E-mail patraho@fis.upv.es.
† Universidad Politécnica de Valencia.
‡ Universitat de Valencia.
§ Universitat Jaume I.

10.1021/jp035778w CCC: $25.00
Published on Web 11/01/2003

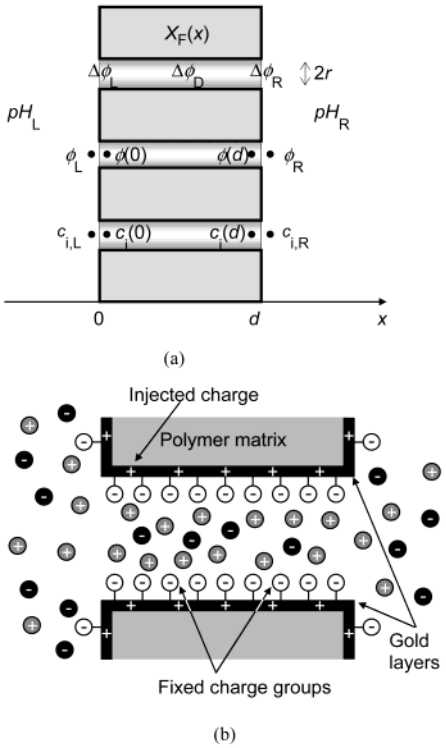

Figure 1. Sketch of the membrane system (a) and the nanopore (b). The membrane extends from $x = 0$ to d and consists of a porous polymeric support with a gold layer deposited onto the pore walls and the faces of the polymeric matrix. The pore radius after plating is r. The bathing solutions contain the ionic form of the fully dissociated drug, the anions and cations of the supporting electrolyte, and the hydrogen and hydroxide. $c_{i,j}$ is the concentration of the species i in the bulk of the bathing solution j; ϕ_j and pH_j refer to the electric potential and the pH value of the solution j; and $c_i(x)$ and $\phi(x)$ are the local concentration of species i and the local electric potential within the pore. $\Delta\phi_L = \phi(0) - \phi_L$ and $\Delta\phi_R = \phi_R - \phi(d)$ denote the Donnan potential differences through the left and right membrane/solution interfaces, and $\Delta\phi_D = \phi(d) - \phi(0)$ is the diffusion potential within the pore. Finally, $X_F(x)$ is the total fixed charge concentration at position x.

deposited onto the pore walls and membrane faces of the polymeric matrix. Commercially available microporous polycarbonate filters with monodisperse cylindrical pores of radius r after plating (see Figure 1b) are normally used.[11−16,31,32,39−44] The nanopore membrane separates two solutions containing the ionic form of the fully dissociated drug, the anions and cations of the supporting electrolyte, and hydrogen and hydroxyde ions. The solutions are assumed to be perfectly stirred, and the whole system is isothermal. $c_{i,j}$ is the concentration of the species i in the bulk of the bathing solution j (j = L for the left and j = R for the right bathing solutions), and ϕ_j and pH_j (j = L and R) refer to the electric potential and the pH value of the solution j, respectively. $c_i(x)$ and $\phi(x)$ are the local concentration of the species i and the electric potential within the pore (see Figure 1a). The potential drops $\Delta\phi_L = \phi(0) - \phi_L$ and $\Delta\phi_R = \phi_R - \phi(d)$, denote, respectively, the Donnan potential differences through the left and right interfaces, and $\Delta\phi_D = \phi(d) - \phi(0)$ is the diffusion potential within the pore. The ionic selectivity of the membrane is achieved by chemisorption of ionizable groups (negatively charged in Figure 1b) onto the gold layers[11−16,31,40,41] and/or by injecting excess charge in these layers via an applied electric potential[16,31,42] (Figure 1b). This excess charge can be either positive (as in Figure 1b) or negative, depending on the sign of the electric potential applied to the gold layers. Finally, $X_F(x)$ is the total membrane fixed charge concentration at position x in Figure 1, parts a and b.

The basic equations governing the ionic transport through the membrane are the Nernst−Planck equations[30,33,35]

$$J_i = -D_i\frac{dc_i}{dx} - z_i D_i c_i \frac{F}{RT}\frac{d\phi}{dx} \quad (1)$$

the electroneutrality condition for the solution in the membrane pore

$$\sum_i z_i c_i + X_F = 0 \quad (2)$$

the condition of zero current

$$\sum_i z_i J_i = 0 \quad (3)$$

and the dissociation equilibrium for the H^+ and OH^- ions

$$c_{H^+}c_{OH^-} = K_W \quad (4)$$

In eqs 1−4, z_i, D_i, and J_i denote respectively the charge number, the diffusion coefficient, and the flux of species i, $K_W = 10^{-14}$ M^2, and constants F, R, and T have their usual meaning.[1]

Substitution of eq 4 in eqs 1 for $i = H^+$ and OH^- leads to

$$J_{OH^-} = -\frac{D_{OH^-}}{D_{H^+}}\frac{K_W}{c_{H^+}^2}J_{H^+} \quad (5)$$

External and membrane solution concentrations are connected through the Donnan equilibrium conditions,[1,35] at interfaces $x = 0$ and $x = d$

$$c_i(0) = c_{i,L}\exp\left(-\frac{z_i F}{RT}\Delta\phi_L\right) \quad (6)$$

$$c_i(d) = c_{i,R}\exp\left(\frac{z_i F}{RT}\Delta\phi_R\right) \quad (7)$$

where the specific ionic partition coefficients between the external and the membrane solutions[1] are assumed to be unity (this assumption should be revised if solute partition effects due to hydrophilic/hydrophobic interactions are incorporated into the model[12,13,31]).

The inner membrane concentrations $c_i(0)$ and $c_i(d)$ and the Donnan potential differences $\Delta\phi_L$ and $\Delta\phi_R$ can be obtained from eqs 2, 6, and 7 in terms of the species concentrations in the bathing solutions.

Equations 1−7 constitute a set of algebraic and differential equations for the ionic fluxes, the electric potential and the ionic concentrations subject to the boundary conditions $c_i(0)$, $c_i(d)$, and $\phi(0)$. The solution to this boundary value problem can be found using an iterative scheme, e.g., the shooting or the relaxation methods.[45] However, we have preferred to estimate the ionic fluxes (assuming that they are approximately constant through the nanopore) using the Goldman constant field (GCF) approximation which considers that the electric field $-d\phi/dx$ within the membrane is constant and approximately equal to $-\Delta\phi_D/d$.[34] The resulting fluxes can then be written in closed form and reproduce the qualitative trends of the model, especially when small pH gradients are applied to the membrane.[8,46]

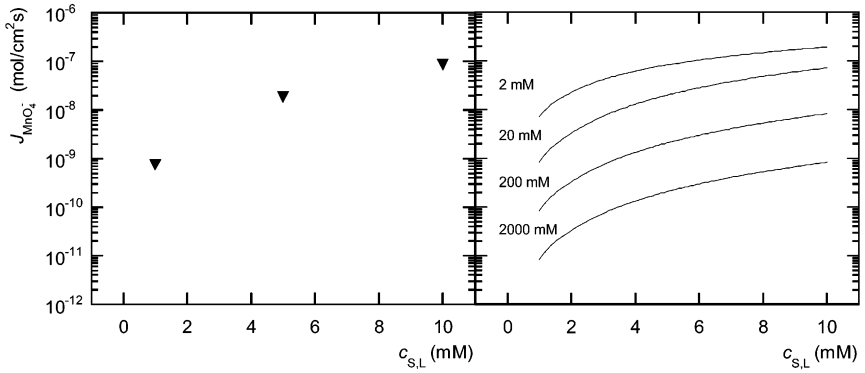

Figure 2. Flux of MnO_4^- vs $KMnO_4$ concentration in bathing solution L through a PCTE/Au/Cl^- membrane with pore radius $r \approx 15$ nm and thickness $d = 6$ μm: experiments (a) from ref 15 and theoretical curves (b) parametric in X_A obtained with infinite dilution diffusion coefficients.

Assuming that all the ionic fluxes are constant and using the GCF approximation, the direct integration of eqs 1 yields

$$J_i \approx \frac{z_i F}{RT}\frac{D_i \Delta\phi_D}{d}\frac{c_i(0)\exp(-z_i F\Delta\phi_D/RT) - c_i(d)}{1-\exp(-z_i F\Delta\phi_D/RT)} \quad (8)$$

Substituting eq 8 into eq 3 for each ion

$$\sum_i \frac{z_i^2 F}{RT}\frac{D_i \Delta\phi_D}{d}\frac{c_i(0)\exp(-z_i F\Delta\phi_D/RT) - c_i(d)}{1-\exp(-z_i F\Delta\phi_D/RT)} = 0 \quad (9)$$

When $z_i = \pm 1$, eq 9 can be solved analytically for $\Delta\phi_D$ to give

$$\Delta\phi_D = \frac{RT}{F}\frac{\sum_k D_k c_k(0) + \sum_l D_l c_l(d)}{\sum_k D_k c_k(d) + \sum_l D_l c_l(0)} \quad (10)$$

where k and l denote the cationic and anionic species present in the problem, respectively. For higher charge numbers, eq 9 can still be solved using a simple numerical procedure like the Newton−Raphson method.[45] Once $\Delta\phi_D$ has been determined, the ion fluxes of eq 8 and the membrane potential

$$\Delta\phi_M = \Delta\phi_L + \Delta\phi_D + \Delta\phi_R = \frac{RT}{F}\log\left(\frac{c_{i,L}}{c_i(0)}\right)^{1/z_i} + \Delta\phi_D + \frac{RT}{F}\log\left(\frac{c_i(d)}{c_{i,R}}\right)^{1/z_i} \quad (11)$$

can be also obtained.

III. Results and Discussion

We have compared the results provided by the theoretical model with recent experimental data by Stroeve and co-workers[15,16] and Martin and co-workers[14,31,32] for gold-coated nanoporous polycarbonate track etched (PCTE) membranes. These studies consider a broad range of experimental situations and are therefore suitable to check the model predictions.

Figures 2 and 3 are concerned with experiments obtained for membranes with Cl^- ions adsorbed onto the gold layers.[14,15,31,32] In Figure 2, a gold-coated PCTE membrane with hydraulic pore radius $r \approx 15$ nm and thickness $d = 6$ μm separated an aqueous $KMnO_4$ solution (left) from a pure water solution (right).[15] Prior to the experiments, the membrane was immersed in a 1 mM KCl solution to provide a source for the Cl^- ions adsorbed on the gold layers. The experimental points in Figure 2a correspond to the flux of the permanganate anion ($J_{MnO_4^-}$) as a function of the $KMnO_4$ concentration $c_{S,L}$. For these experimental conditions, the ionic concentrations at $x = 0$ and d can be calculated from eqs 2, 6, and 7 for $i = K^+$ and MnO_4^- to give

$$c_{MnO_4^-}(0) = \frac{\sqrt{{X_A}^2 + 4{c_{S,L}}^2} - X_A}{2}, \quad c_{MnO_4^-}(d) \approx 0 \quad (12a)$$

$$c_{K^+}(0) = \frac{\sqrt{{X_A}^2 + 4{c_{S,L}}^2} + X_A}{2}, \quad c_{K^+}(d) \approx X_A \quad (12b)$$

where we have assumed that the Cl^- ions adsorbed to the gold layers are homogeneously distributed on the pore walls giving rise to a uniform (negative) fixed charge concentration $X_F = -X_A$. The flux $J_{MnO_4^-}$ can then be computed from eq 8

$$J_{MnO_4^-} \approx -\frac{F}{RT}\frac{D_{MnO_4^-}\Delta\phi_D}{d}\frac{c_{MnO_4^-}(d)\exp(-F\Delta\phi_D/RT) - c_{MnO_4^-}(0)}{1-\exp(-F\Delta\phi_D/RT)} \quad (13)$$

where the diffusion potential (see eq 10) is

$$\Delta\phi_D \approx \frac{RT}{F}\log\frac{D_{K^+}c_{K^+}(0) + D_{MnO_4^-}c_{MnO_4^-}(d)}{D_{K^+}c_{K^+}(d) + D_{MnO_4^-}c_{MnO_4^-}(0)} \quad (14)$$

The results obtained using eqs 13−14 with the concentrations of eqs 12 are shown in Figure 2b (continuous curves). The curves are parametric in the fixed charge concentration X_A and have been obtained with the infinite dilution diffusion coefficients $D_{K^+} = 1.95\ 10^{-5}$ cm^2/s and $D_{MnO_4^-} = 10^{-5}$ cm^2/s.[47] As expected, $J_{MnO_4^-}$ increases with increasing $c_{S,L}$. The theoretical model accounts for the experimental data if $X_A \approx 20$ mM. This gives the order of magnitude of the effective fixed charge concentration in the nanoporous membranes. Because $X_A \approx 20$ mM is of the order of $c_{S,L}$, then $F\Delta\phi_D/RT \ll 1$ and eq 13 can be approximated in the form

$$J_{MnO_4^-} \approx \frac{D_{MnO_4^-}c_{MnO_4^-}(0)}{d} = \frac{D_{MnO_4^-}}{d}\frac{\sqrt{{X_A}^2 + 4{c_{S,L}}^2} - X_A}{2} \quad (15)$$

which shows clearly the dependence of $J_{MnO_4^-}$ on X_A and $c_{S,L}$.

It is also possible to estimate the surface density σ of Cl^- ions adsorbed onto the pore walls from the equation[48]

$$\sigma 2\pi r = F X_A \pi r^2 \quad (16)$$

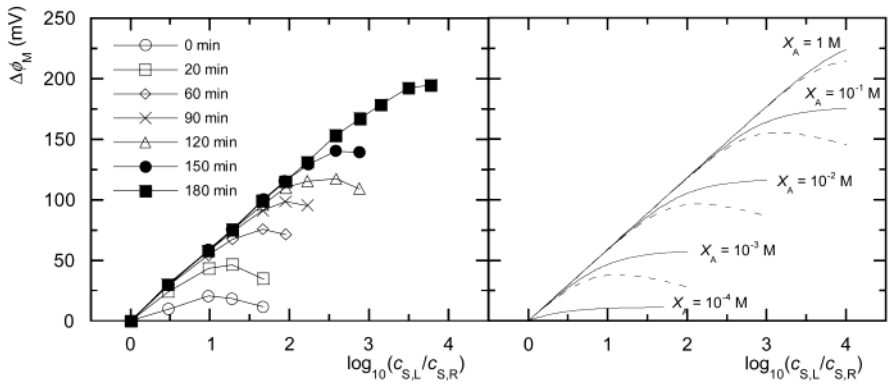

Figure 3. Membrane potential of PCTE/Au/Cl^- membranes with $d = 6\ \mu$m and different plating times vs the KCl concentration ratio with $c_{S,R} = 0.1$ mM: experimental data (a) from ref 14 and theoretical results (b) using the GCF approximation (continuous curves) and the TMS theory (dashed curves). The calculations assume that the membrane fixed charge X_A increases with increasing the plating time.

Substituting $r \approx 15$ nm and $X_A \approx 20$ mM in eq 16, we obtain $\sigma \approx 1.5\ \mu$C/cm^2. This is a reasonable estimation for the adsorbed surface charge density (see, e.g., refs 48 and 49).

In the data reported in Figure 3, a gold-coated polycarbonate filter with $d \approx 6\ \mu$m separated two KCl solutions.[14,31,32] The concentration $c_{S,R}$ in the right bathing solution was kept constant to 0.1 mM, and the concentration $c_{S,L}$ in the left bathing solution was varied from 0.1 mM to 1 M. The experimental curves in Figure 3a show the membrane potential $\Delta\phi_M = \phi_R - \phi_L$, measured with membranes prepared with different plating times, as a function of $\log_{10}(c_{S,L}/c_{S,R})$. The membranes display an ideal cation-permselective behavior, characterized by the linear dependence of $\Delta\phi_M$ with $\log_{10}(c_{S,L}/c_{S,R})$, for small $c_{S,L}/c_{S,R}$ ratios. At higher $c_{S,L}/c_{S,R}$ ratios, however, the curves deviate from linearity and attain a maximum $\Delta\phi_{M,max}$. As plating time increases, $\Delta\phi_{M,max}$ also increases, and the position of the maxima shifts to higher $c_{S,L}/c_{S,R}$ ratios.

The continuous curves in Figure 3b have been calculated using the GCF approximation. In this case, the membrane potential (see eqs 10 and 11 for $k = K^+$ and $l = Cl^-$) is

$$\Delta\phi_M \approx \frac{RT}{F}\left(\log\frac{c_{S,L}}{c_{S,R}}\frac{c_{K^+}(d)}{c_{K^+}(0)} + \log\frac{D_{K^+}c_{K^+}(0) + D_{Cl^-}c_{Cl^-}(d)}{D_{K^+}c_{K^+}(d) + D_{Cl^-}c_{Cl^-}(0)}\right) \quad (17)$$

where

$$c_{Cl^-}(0) = \frac{\sqrt{X_A^2 + 4c_{S,L}^2} - X_A}{2}, \qquad c_{Cl^-}(d) = \frac{\sqrt{X_A^2 + 4c_{S,R}^2} - X_A}{2} \quad (18a)$$

$$c_{K^+}(0) = \frac{\sqrt{X_A^2 + 4c_{S,L}^2} + X_A}{2}, \qquad c_{K^+}(d) = \frac{\sqrt{X_A^2 + 4c_{S,R}^2} + X_A}{2} \quad (18b)$$

In eqs 18 we have assumed (as in Figure 2) that a uniform negative fixed charge concentration $X_F = -X_A$ exists on the pore walls due to the Cl^- ions adsorbed on the gold layers. According to eq 16, the fixed charge concentration X_A increases with the surface density of Cl^- ions adsorbed on the gold layers and, hence, with increasing the plating time. Therefore, we have plotted in Figure 3b a set of curves parametric in X_A and introduced, for the sake of simplicity, the infinite dilution values $D_{K^+} = 1.95 \times 10^{-5}$ cm^2/s and $D_{Cl^-} = 2.03 \times 10^{-5}$ cm^2/s for the ionic diffusion coefficients.[47] The theoretical model with the GCF assumption reproduces the experimental trends in the linear region of the curves. In this region, eq 17 can be approximately written in the form

$$\Delta\phi_M \approx \frac{RT}{F}\log\frac{c_{S,L}}{c_{S,R}} = 2.30\frac{RT}{F}\log_{10}\frac{c_{S,L}}{c_{S,R}} \quad (19)$$

which yields a straight line of slope 59 mV for $T = 298$ K. The deviations from linearity observed for higher values of $c_{S,L}/c_{S,R}$ can also be explained by the model. However, the GCF approximation fails when attempting to reproduce the maxima in the experimental data. This effect can be accounted for by integrating eqs 1−3 directly instead of using the GCF approximation (the so-called TMS theory[1]). For $i = K^+$ and Cl^-, it is possible to obtain an analytical equation for the membrane potential[1] as

$$\Delta\phi_M \approx \frac{RT}{F}\left(\log\frac{c_{S,L}}{c_{S,R}}\frac{c_{K^+}(d)}{c_{K^+}(0)} + \Gamma\log\frac{\sqrt{1 + (2c_{S,R}/X_A)^2} + \Gamma}{\sqrt{1 + (2c_{S,L}/X_A)^2} + \Gamma}\right), \qquad \Gamma \equiv \frac{D_{Cl^-} - D_{K^+}}{D_{Cl^-} + D_{K^+}} \quad (20)$$

The dashed curves in Figure 3b correspond to the results obtained with eq 20 for $D_{K^+} = 10^{-5}$ cm^2/s and $D_{Cl^-} = 2 \times 10^{-5}$ cm^2/s. Note that in order to reproduce the experimental trends the counterion diffusion coefficient must be reduced respect to that of the co-ion, as is usually the case in ion exchange membranes[35] due to the attractive interaction between the counterion and the membrane fixed charges.

Figures 4 and 5 refer to the transport of ionic drugs through gold-coated PCTE nanoporous membranes with self-assembled monolayers of $HS(CH_2)_{10}$-COOH formed onto gold as pH-dependent ionizable surface groups. In the experiments shown in Figure 4a,[15] a membrane with hydraulic pore radius of $r \approx 8$ nm and thickness of $d = 6\ \mu$m separated two bathing solutions containing a mixture of sodium benzenesulfonate (SBS) and NaCl (left solution) and pure NaCl (right solution). The pH of the external solutions was adjusted to be equal in both compartments ($pH_L = pH_R \equiv pH$) by the addition of either HCl or NaOH. The flux of the benzenesulfonate anion J_{BS^-} vs the external pH is shown in Figure 4a, where all experimental points correspond to the SBS concentrations $c_{D,L} = 1$ mM and $c_{D,R} \approx 0$. Because the pK_a of SBS is approximately 0.7, the drug is

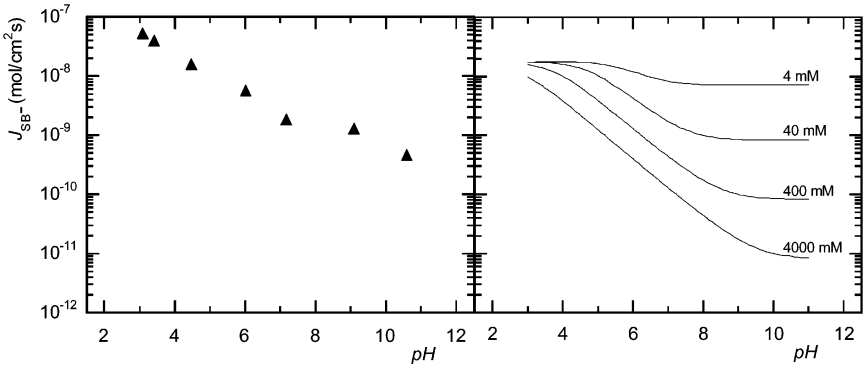

Figure 4. Flux of benzenesulfonate (SB^-) vs $pH \equiv pH_L = pH_R$ through a PCTE/Au/HS$(CH_2)_{10}$−COOH membrane with $r \approx 8$ nm and $d = 6$ μm. The sodium benzenesulfonate (SBS) concentrations were $c_{D,L} = 1$ mM and $c_{D,R} \approx 0$. NaCl was added to solutions L and R in order to keep the ionic strength equal to $s_j = 2$ mM. Experimental data (a) from ref 15 and theoretical curves (b) parametric in X_{CT}.

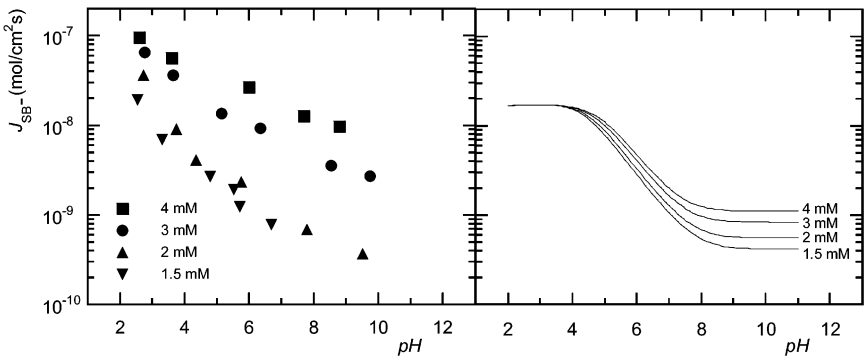

Figure 5. Effect of the ionic strength on the flux of SB^- vs $pH \equiv pH_L = pH_R$ through a PCTE/Au/HS$(CH_2)_{10}$-COOH membrane with $r \approx 5.5$ nm and $d = 6$ μm. The concentrations of SBS were $c_{D,L} = 1$ mM and $c_{D,R} \approx 0$. Experimental data (a) from ref 15 and theoretical curves (b).

completely dissociated in the range of pH studied. The concentrations of NaCl in the left and right compartments were adjusted to keep the same ionic strength $s_j = 2$ mM (j = L and R) in the solutions. The experiment shows that J_{BS^-} decreases with increasing the pH, being approximately 110 times higher for pH = 3.1 than for pH = 10.6.[15]

For the experimental conditions described above, the concentrations of the different ionic species in the bulk solutions are

$$c_{H^+,j} = 10^{-pH_j}, \quad c_{OH^-,j} = K_W/c_{H^+,j}, \quad c_{BS^-,j} = c_{D,j}, \quad c_{Na^+,j} = s_j - c_{H^+,j}, \quad c_{Cl^-,j} = s_j - c_{BS^-,j} - c_{OH^-,j}, \quad j = \text{L and R} \tag{21}$$

The nanopores contain ionizable carboxylic groups attached to the pore walls. We assume that these groups are homogeneously distributed on the pore surface. The neutral HS$(CH_2)_{10}$-COOH and dissociated HS$(CH_2)_{10}$-COO^- forms of the carboxylic groups are in equilibrium with the H^+ ions in the membrane solution according to the scheme

$$HS(CH_2)_{10} - COOH \overset{K_N}{\rightleftharpoons} HS(CH_2)_{10} - COO^- + H^+ \tag{22}$$

where K_N is the equilibrium constant for the dissociation reaction. Note that the hydrogen concentration in the membrane solution can be significantly different from that in the bathing solution because of the membrane fixed charges.[8]

From eq 22, we obtain

$$10^{-pK_a} = K_N = \frac{X_C^N c_{H^+}}{X_C^0} \tag{23}$$

where X_C^N and X_C^0 are respectively the concentrations of the negative HS$(CH_2)_{10}$-COO^- and neutral HS$(CH_2)_{10}$-COOH carboxylic groups. From eq 23 and defining $X_{CT} = X_C^N + X_C^0$, where X_{CT} is the total concentration of carboxylic groups, the membrane fixed charge concentration (with its sign) is

$$X_F = -X_C^N = -\frac{X_{CT}}{1 + c_{H^+}/K_N} \tag{24}$$

Combining eqs 2, 6, 7, and 24, the following equations are obtained

$$\left(1 + \frac{c_{Na^+,j}}{c_{H^+,j}}\right)\left(u_j - \frac{1}{u_j}\right) - \frac{X_{CT}/c_{H^+,j}}{1 + c_{H^+,j}u_j/K_N} = 0, \quad j = \text{L and R} \tag{25}$$

where $u_L \equiv c_{H^+}(0)/c_{H^+,L}$ and $u_R \equiv c_{H^+}(d)/c_{H^+,R}$. Equation 25 can be readily solved for u_j using a numerical procedure. After determining u_j, concentrations $c_j(0)$ and $c_j(d)$ can be obtained from eqs 6 and 7 in terms of the concentrations of the different species in the bathing solutions. Once all of the concentrations $c_j(0)$ and $c_j(d)$ have been calculated, the diffusion potential

$$\Delta\phi_D \approx \frac{RT}{F} \log \times \frac{D_{Na^+}c_{Na^+}(0) + D_{H^+}c_{H^+}(0) + D_{Cl^-}c_{Cl^-}(d) + D_{OH^-}c_{OH^-}(d) + D_{SB^-}c_{SB^-}(d)}{D_{Na^+}c_{Na^+}(d) + D_{H^+}c_{H^+}(d) + D_{Cl^-}c_{Cl^-}(0) + D_{OH^-}c_{OH^-}(0) + D_{SB^-}c_{SB^-}(0)} \tag{26}$$

and the flux of the SB^- anion

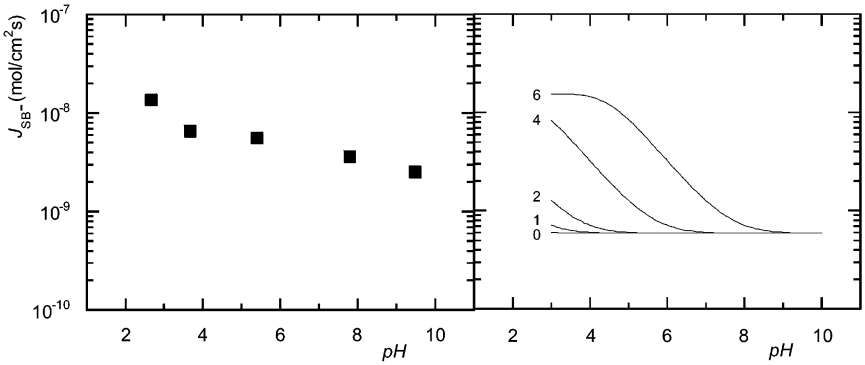

Figure 6. Flux of SB^- vs pH $\equiv$ $pH_L = pH_R$ through a PCTE/Au/HS$(CH_2)_3-SO_3H$ membrane with $r \approx 5.9$ nm and $d = 6$ μm. The concentrations of SBS were $c_{D,L} = 1$ mM and $c_{D,R} \approx 0$, and the ionic strength of the two bathing solutions was 2 mM. Experimental data (a) from ref 15 and theoretical curves (b) parametric in the pK_a of the fixed ionizable groups.

$$J_{SB^-} \approx -\frac{F}{RT}\frac{D_{SB^-}\Delta\phi_D}{d}\frac{c_{SB^-}(d)\exp(-F\Delta\phi_D/RT) - c_{SB^-}(0)}{1-\exp(-F\Delta\phi_D/RT)} \quad (27)$$

are readily obtained.

Figure 4b shows the theoretical results provided by eqs 26 and 27 using the infinite dilution diffusion coefficients $D_{Na^+} = 1.33 \times 10^{-5}$ cm^2/s, $D_{Cl^-} = 2.03 \times 10^{-5}$ cm^2/s, $D_{SB^-} = 10^{-5}$ cm^2/s, $D_{H^+} = 9 \times 10^{-5}$ cm^2/s, and $D_{OH^-} = 4.5 \times 10^{-5}$ cm^2/s.[47] The pK_a of the carboxylic groups in free solution is usually in the range of 3−6, but much higher values have also been reported in self-assembled monolayers formed from thiols on flat gold surfaces and long-chain fatty acids.[15,50] We have used p$K_a = 6$ in the calculations of Figure 4b, where the curves are parametric in the concentration of fixed ionizable groups X_{CT}. If we assume that the carboxylic groups are distributed onto the pore walls with the same surface charge σ as the Cl^- ions in the case of Figure 2, then $X_{CT} \approx 40$ mM from eq 16, which agrees qualitatively with the experimental data in Figure 4a. At low pH (pH $\ll$ pK_a), the carboxylic groups are protonated, and then the flux of SB^- is high. For high pH (pH $\gg$ pK_a), these groups become negatively charged, and the SB^- ions are excluded from the pores.[35] This co-ion exclusion leads to low salt fluxes. It must be emphasized however that the agreement is only qualitative: some discrepancies appear at extremely low and high pH values. For instance, at pH $\approx$ 3.1 the experimental value for the flux of SB^- ions is $J^{exp}_{BS^-} \approx 5 \times 10^{-8}$ mol cm^{-2} s^{-1}, whereas the theoretical model gives only $J^{theo}_{BS^-} \approx 2 \times 10^{-8}$ mol cm^{-2} s^{-1} for $X_{CT} \approx 40$ mM. Also, at pH $\approx$ 10.6, we find $J^{exp}_{BS^-} \approx 5 \times 10^{-10}$ mol cm^{-2} s^{-1}, but $J^{theo}_{BS^-} \approx 8 \times 10^{-10}$ mol cm^{-2} s^{-1} for $X_{CT} \approx 40$ mM. Therefore, the model predicts that the flux of BS^- is approximately 25 times higher for pH = 3.1 than for pH = 10.6, whereas the experiments show that this factor is approximately 100.[15]

The above discrepancies should be ascribed to effects not included in the theoretical model: the changes in the pH of the bathing solutions might affect the effective radius of the nanopores through changes in the monolayer conformation and the salt concentration might also modify the effective pK_a value of the carboxylic groups due to screening effects between fixed charges.[26] Moreover, transport mechanisms other than simple electrodiffusion (e.g., surface diffusion[15]) could be present. It has also been reported that SB^- ions adsorb onto gold, and this fact, together with the adsorption of Cl^- ions, could modify noticeably both the surface charge of the membrane and the effective pore radius. Finally, it should be pointed out that deposition of gold onto the pore walls causes some of the nanopores to close off completely,[31] and then the real pore radii of the nanopores could be higher than those obtained from the experiments using the Hagen-Poiseuille law of capillary flow.[15] In this case, the fluxes of SB^- would be smaller than those in Figure 4a, and then the fixed charge concentration needed to account for the experimental data would be larger (see Figure 4b). For instance, a fixed charge concentration $X_{CT} \approx 200$ mM leads to a J_{BS^-} approximately 100 times higher for pH = 3.1 than for pH = 10.6, which is closer to the experimental findings.

Figure 5 shows the effect of the ionic strength of the bathing solutions on the flux of SB^- through a PCTE/Au/HS$(CH_2)_{10}-$COOH membrane of thickness $d = 6$ mm and pore radius $r \approx 5.5$ nm.[16] The experimental results are given in Figure 5a as a function of $pH_L = pH_R \equiv$ pH and correspond to the SBS concentrations $c_{D,L} = 1$ mM and $c_{D,R} \approx 0$. The theoretical results provided by eqs 21−27 are plotted in Figure 5b. We have introduced the same values for the ionic diffusion coefficients and pK_a of the carboxylic groups as in Figure 4b. Now $X_{CT} \approx 60$ mM, calculated from eq 16 assuming that the carboxylic groups are distributed onto the pore walls with the same surface charge σ as in Figures 2−4. The shape of the theoretical curves in Figure 5b can be interpreted roughly as follows: when pH $\ll$ pK_a, most of the surface carboxylic groups are in protonated form, and the fixed charge concentration of the membrane is nearly zero. The concentration of SB^- ions at the left membrane−solution interface is then relatively high and approximately equal to $c_{D,L}$. Therefore

$$J_{SB^-} \approx -D_{SB^-}\frac{c_{SB^-}(0) - c_{SB^-}(d)}{d} \quad (28)$$

depends hardly on the ionic strength of the solutions. On the contrary, when p$K_a \ll$ pH $<$ 10 most of the fixed carboxylic groups deprotonate and $X_F = -X^N_C \approx -X_{CT}$. In this pH range, eq 25 gives approximately

$$c_{Na^+,j}(u_j - 1/u_j) - X_{CT} \approx 0, j = L,R \quad (29)$$

whereas the concentrations of the ionic species in the bulk solutions are

$$c_{H^+,j} \approx 0, \quad c_{OH^-,j} \approx 0, \quad c_{BS^-,j} = c_{D,j}, \quad c_{Na^+,j} \approx s_j, \quad c_{Cl^-,j} \approx s_j - c_{BS^-,j}, \quad j = L \text{ and } R \quad (30)$$

From eqs 29 and 30, the concentrations of SB^- ions at the membrane-solution interfaces are

$$c_{SB^-}(0) \approx \frac{c_{D,L}}{2s_L}(-X_{CT} + \sqrt{{X_{CT}}^2 + {s_L}^2}), \quad c_{SB^-}(d) \approx 0 \quad (31)$$

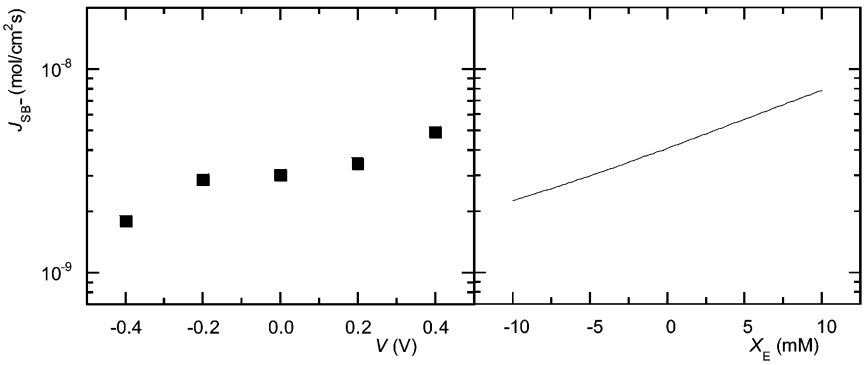

Figure 7. Flux of SB^- vs the electric potential V applied to the gold layers of a PCTE/Au/HS$(CH_2)_{10}-$COOH membrane with $r \approx 4.0$ nm and $d = 6\ \mu$m. The pH of the two bathing solutions was $pH_L = pH_R = 5.68$; the concentrations of SBS were $c_{D,L} = 1$ mM and $c_{D,R} \approx 0$; and the ionic strength was 2 mM. Experimental data (a) from ref 16 and theoretical curves (b) assuming that the voltage applied to the membrane injects an excess charge of concentration X_E.

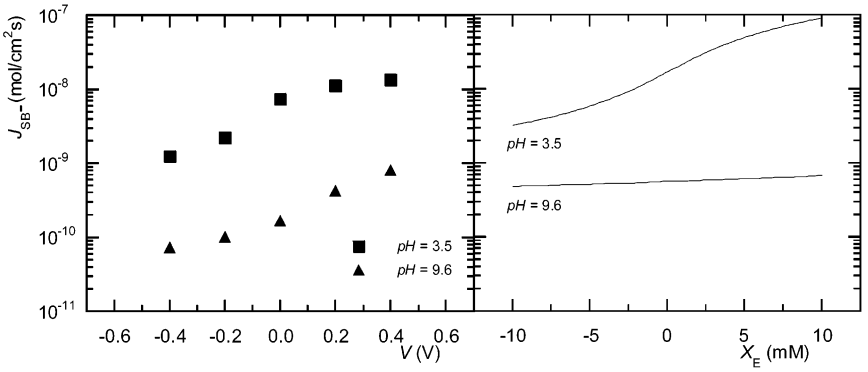

Figure 8. Flux of SB^- vs the electric potential V applied to the gold layers of a PCTE/Au/HS$(CH_2)_{10}-$COOH membrane with $r \approx 5.2$ nm and $d = 6\ \mu$m. The pH of the two bathing solutions was $pH_L = pH_R = 3.5$ (upper curve) and 9.6 (lower curve); the concentrations of SBS were $c_{D,L} = 1$ mM and $c_{D,R} \approx 0$; and the ionic strength was 2 mM. Experimental data (a) from ref 16 and theoretical curves (b) assuming that the voltage applied to the membrane injects an excess charge of concentration X_E.

Equation 31 shows that $c_{SB^-}(0)$ (and then J_{BS^-}) increases with the ionic strength of the left bulk bathing solution. This is in qualitative agreement with the experimental trends of Figure 5a. However, the experiments show that J_{BS^-} depends on the ionic strength of the bathing solutions even at low pH. Also, we see that, at a fixed pH, the differences between the experimental fluxes J_{BS^-} for the different ionic strengths shown in Figure 5a are more pronounced than those predicted by the theory in Figure 5b. This gives support to the hypothesis of simultaneous SB^- and Cl^- adsorption onto the pore walls (see the above discussion concerning Figure 4).

The results of Figure 6a show the effect of the pK_a of the ionizable groups on the flux of SB^-. The system was identical to that of Figure 4a, but now a PCTE/Au/HS$(CH_2)_3-SO_3H$ membrane with hydraulic pore radius $r = 5.9$ nm and thickness $d = 6\ \mu$m[16] is used. The experiments show that the variation of J_{BS^-} with the pH of the solutions in now less pronounced than that observed in Figure 4a using a PCTE/Au/HS$(CH_2)_{10}-$COOH membrane.

The theoretical results in Figure 6b have been calculated from eq 27 with $X_{CT} \approx 50$ mM for the total concentration of sulfonic groups and the same values for the model parameters as in Figures 4 and 5. The curves are parametric in the pK_a of the fixed ionizable groups. We see now that relatively low pK_a values can reproduce the experimental trends, as could be anticipated from the fact that the sulfonic groups present a pK_a lower than that of the carboxylic groups.[35] Note also that the fluxes predicted by the theory are significantly lower than the experimental ones. This could indicate that the sulfonic groups are distributed onto the pore walls with a lower surface density than that of the carboxylic groups, contrary to our assumption for X_{CT}.

Figures 7−9 show the effect of injecting excess charge in the gold layers of the membrane via an applied electric potential.[14,16,31,32,42] Figures 7 and 8 give the flux of SB^- through PCTE/Au/HS$(CH_2)_{10}-$COOH membranes vs the electric potential V applied to the gold layers.[16] As in Figures 4−6, the membrane separated two solutions containing a mixture of SBS with concentrations $c_{D,L} = 1$ mM and $c_{D,R} \approx 0$, and the ionic strength (NaCl) was kept constant to 2 mM in the bathing solutions. The experimental points correspond to nanopores with pore radii $r \approx 4.0$ nm (Figure 7a) and $r \approx 5.2$ nm (Figure 8a). In each set of measurements, the pH of the two bathing solutions was kept constant to 5.68 (Figure 7a), 3.5 (Figure 8a, upper curve), and 9.6 (Figure 8a, lower curve). For this system, we assume that the excess charge introduced by the applied potential increases the fixed charge concentration X_E proportionally to V. With this assumption, eqs 24 and 25 become

$$X_F = X_E - X_C^N = X_E - \frac{X_{CT}}{1 + c_{H^+}/K_N} \tag{32}$$

and

$$\left(1 + \frac{c_{Na^+,j}}{c_{H^+,j}}\right)\left(u_j - \frac{1}{u_j}\right) + \frac{X_E}{c_{H^+,j}} - \frac{X_{CT}/c_{H^+,j}}{1 + c_{H^+,j}u_j/K_N} = 0, \quad j = \text{L and R} \tag{33}$$

where $u_L \equiv c_{H^+}(0)/c_{H^+,L}$ and $u_R \equiv c_{H^+}(d)/c_{H^+,R}$.

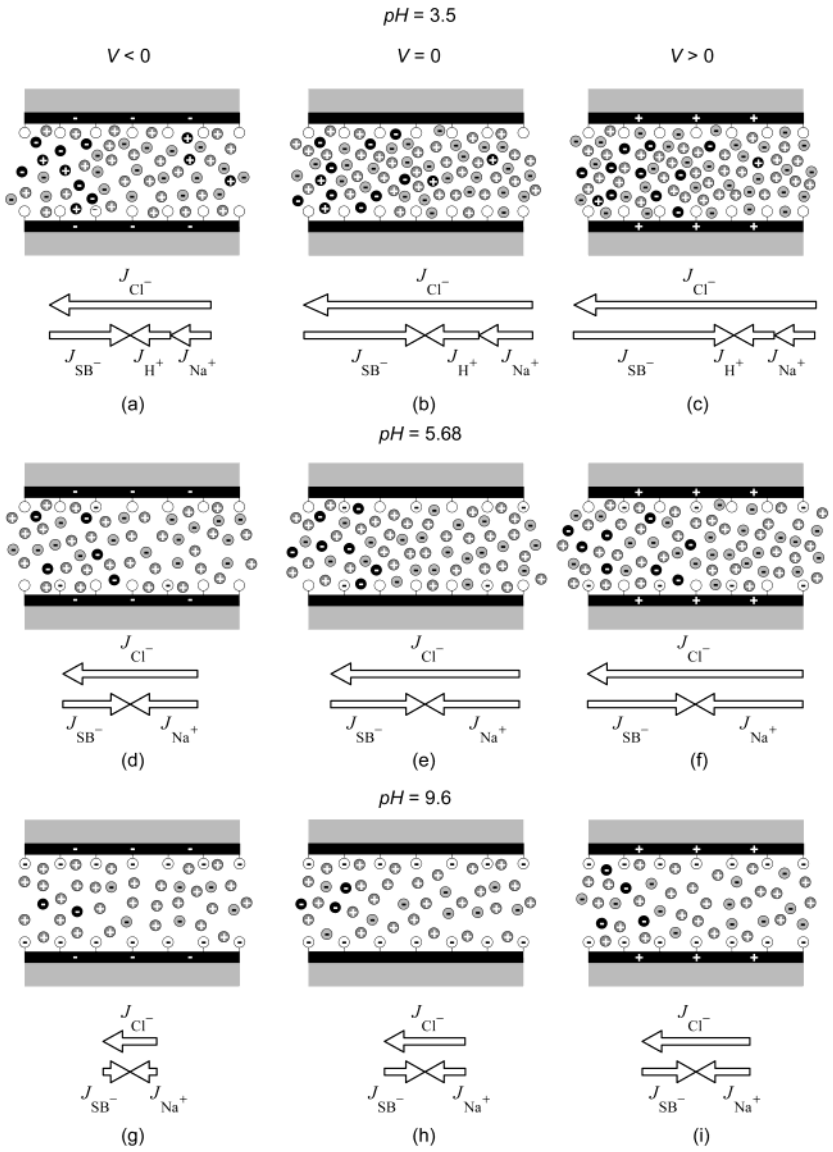

Figure 9. Cartoon showing schematically the nanopore walls and the inside solution (not to scale) under different pH and voltage conditions. The size of the arrows shows the magnitude of the fluxes (not to scale). Black spheres denote the SB^- (−) and the hydrogen (+) ions; shaded spheres are the Cl^- (−) and the Na^+ (+) ions; and white spheres refer to the charged (−) and neutral (blank) forms of the carboxylic groups attached to the gold layers.

Figures 7b and 8b show the theoretical fluxes of SB^- calculated from eqs 27−33 using the same values for the model parameters as in Figures 4 and 5. Again, we estimate $X_{CT} \approx 75$ mM (Figure 7b) and $X_{CT} \approx 60$ mM (Figure 8b) from eq 16 for $r = 4.0$ and 5.2 nm, respectively, assuming that the fixed charge groups are distributed onto the gold layers with the same surface density as in Figures 2−6. The cartoon in Figure 9 tentatively shows the nanopore walls and the inside solution for the experiments in Figures 7 and 8. When pH = 3.5 < p$K_a \approx 6$ (upper figure, cases a−c), the carboxylic groups are in neutral form. Therefore, for $V = 0$ (case b), the membrane fixed charge is zero. If $V < 0$ (case a), the nanopore becomes negatively charged, and the anions are then excluded from the inner solution (J_{BS^-} decreases). On the contrary, for $V > 0$ (case c), the nanopore fixed charge becomes positive, and the anions can enter the inner solution (J_{BS^-} attains its highest value). Note that, if this membrane were to separate two solutions of the same binary electrolyte, the flux would attain a maximum near the isoelectric point ($V = 0$) because of the condition of zero electric current, as it has been experimentally verified in amphoteric membranes.[51,52] The behavior shown in the upper curve of Figure 8a results from the particular experimental conditions imposed to the system: the concentration of Cl^- at the right membrane/solution interface is always twice that at the left one, and this leads to a flux of Cl^- opposite to the flux of SB^-. Therefore, the condition of zero electric current makes the flux of SB^- to increase at $V > 0$. In the case of pH ≈ 5.68 ≈ p$K_a \approx 6$ (middle figure, cases d−f), only a fraction of the carboxylic groups are in charged form when $V = 0$ (case e). If $V < 0$ (case d), protons enter within the nanopore, the pH of the inner solution becomes lower than that of the outer solution, and then more fixed groups become protonated. However, the net negative charge of the nanopore is higher (in absolute value) than in the case $V = 0$, and thus, J_{BS^-} decreases. For $V > 0$ (case f), protons are excluded from the inner solution, and carboxylic groups become deprotonated. Nevertheless, the positive electric potential applied makes the net negative charge of the membrane lower than that for $V = 0$, and therefore, J_{BS^-} increases. Finally, in the case of pH = 9.6 > p$K_a \approx 6$ (lower figure, cases g−i), all of the fixed carboxylic groups are negatively charged. For $V < 0$ (case g), the net negative charge in the nanopore is high, and J_{BS^-} attains its lowest value. For V

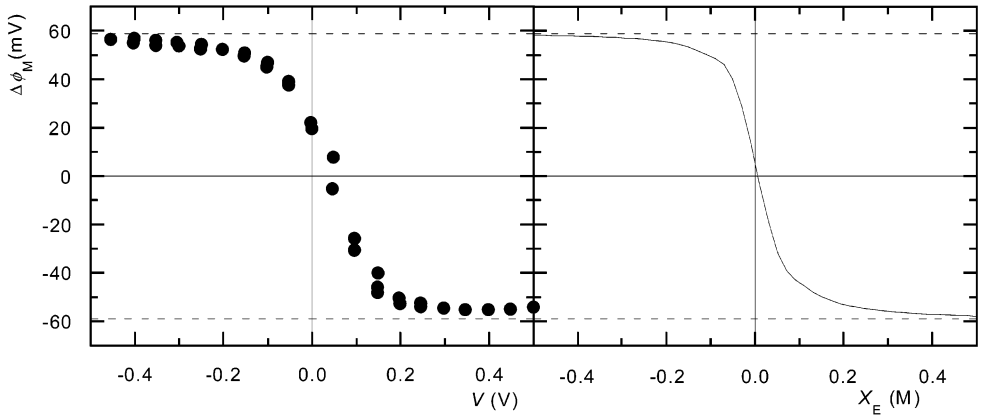

Figure 10. Membrane potential of a PCTE/Au membrane with $r \approx 1.1$ nm and $d = 6$ μm vs the electric potential V applied to the gold layers. The membrane separated two KF solutions of concentrations $c_{S,L} = 10$ mM and $c_{S,R} = 1$ mM. Experimental data (a) from refs 14, 31, and 32 and theoretical curves (b) assuming that the voltage applied to the membrane injects an excess charge of concentration X_E.

$= 0$ (case h) and $V > 0$ (case i), the negative charge of the nanopore gradually decreases, and, consequently, J_{BS^-} increases. Note the correspondence between the size of the arrows denoting the magnitude of the fluxes in Figure 9 and the results of Figures 7 and 8.

The results depicted in Figure 10 constitute an additional test of the theoretical model. In this experiment, a gold-coated polycarbonate filter with pore radius $r = 1.1$ nm and $d \approx 6$ μm separated two KF solutions with concentrations $c_{S,L} = 10$ mM and $c_{S,R} = 1$ mM at pH approximately neutral. Figure 10a shows the experimental membrane potential vs the electric potential applied to the pore walls.[14,31,32] The model calculations are plotted in Figure 10b assuming again that the voltage applied to the gold layers gives rise to a fixed charge X_E proportional to V. Because F^- does not adsorb to gold,[14] the net charge of the nanopore is assumed to be zero for $V = 0$. We have used the infinite dilution diffusion coefficients $D_{K^+} = 1.95 \times 10^{-5}$ cm^2/s and $D_{F^-} = 1.47 \times 10^{-5}$ cm^2/s in the calculations.[47] With these assumptions, the membrane fixed charge concentration becomes now $X_F = X_E$ and the electroneutrality condition within the nanopore yields

$$c_{K^+} - c_{F^-} + X_E = 0 \tag{34}$$

Finally, the membrane potential (eqs 10 and 11 for $k = K^+$ and $l = F^-$) is

$$\Delta\phi_M \approx \frac{RT}{F}\left(\log\frac{c_{S,L}}{c_{S,R}}\frac{c_{K^+}(d)}{c_{K^+}(0)} + \log\frac{D_{K^+}c_{K^+}(0) + D_{F^-}c_{F^-}(d)}{D_{K^+}c_{K^+}(d) + D_{F^-}c_{F^-}(0)}\right) \tag{35}$$

where the concentrations at the inner membrane-solution interfaces (eqs 2, 6, and 7) are

$$c_{F^-}(0) = \frac{\sqrt{X_E^2 + 4c_{S,L}^2} + X_E}{2}, \qquad c_{F^-}(d) = \frac{\sqrt{X_E^2 + 4c_{S,R}^2} + X_E}{2} \tag{36a}$$

$$c_{K^+}(0) = \frac{\sqrt{X_E^2 + 4c_{S,L}^2} - X_E}{2}, \qquad c_{K^+}(d) = \frac{\sqrt{X_E^2 + 4c_{S,R}^2} - X_E}{2} \tag{36b}$$

Remarkably, the results of Figure 10a show that the nanopore can behave as a cation ($V < 0$) or an anion ($V > 0$) selective membrane. The model calculations correctly describe the changes of the membrane potential with the applied potential V, what gives support to our assumption concerning X_E and V (see also the results in Figures 7 and 8).

In summary, we have presented a simple model accounting for the ion transport and selectivity of pH-switchable nanopore membranes with fixed charges. On the basis of a reduced number of assumptions, the theoretical results provide qualitative explanations for a broad range of previous experimental data concerning fluxes and membrane potential obtained under different conditions. Also, the model employed emphasizes clearly which are the main characteristics that allow a relatively simple description of these membranes.

Acknowledgment. Financial support from the CICYT, Ministerio de Ciencia y Tecnología (Projects MAT2002-00646 and BFM2001-3293), Fundació Caixa-Castelló (Project P1-1B2001-20), and the Fondo Europeo para el Desarrollo Regional (FEDER) is gratefully acknowledged.

References and Notes

(1) Lakshminarayanaiah, N. *Equations of Membrane Biophysics*; Academic Press: New York, 1984.

(2) Schultz, S. G. *Basic Principles of Membrane Biophysics*; Cambridge University Press: Cambridge, 1980.

(3) Barboiu, M.; Guizard, C.; Luca, C.; Albu, B.; Hovnanian, N.; Palmeri, J. *J. Membr. Sci*. **1999**, *161*, 193−206.

(4) Minagawa, M.; Tanioka, A.; Ramírez P.; Mafé, S. *J. Colloid Interface Sci*. **1997**, *188*, 176−182.

(5) Chen, J.; Minoura, N.; Tanioka, A. *Polymer* **1994**, *35*, 2853−2856.

(6) Åkerman, S.; Viinikka, P.; Svarfvar, B.; Järvinen, K.; Kontturi, K.; Nasman, J.; Urtti, A.; Paronen, P. *J. Controlled Release* **1998**, *50*, 153−166.

(7) Jimbo, T.; Ramírez, P.; Tanioka, A.; Mafé, S.; Minoura, N. *J. Colloid Interface Sci.* **2000**, *225*, 447−454.

(8) Ramírez, P.; Alcaraz, A.; Mafé, S.; Pellicer, J. *J. Membr. Sci*. **1999**, *161*, 143−153.

(9) Aguilella, V. M.; Kontturi, K.; Murtomäki, L.; Ramírez, P. *J. Controlled Release* **1994**, *32*, 249−257.

(10) Rojanasakul, Y.; Robinson, J. R. *Int. J. Pharm.* **1989**, *55*, 237−246.

(11) Lee, S. B.; Martin, C. R. *Anal. Chem.* **2001**, *73*, 768−775.

(12) Lee, S. B.; Martin, C. R. *Chem. Mater*. **2001**, *13*, 3236−3244.

(13) Hulteen, J. C.; Jirage, K. B.; Martin, C. R. *J. Am. Chem. Soc.* **1998**, *120*, 6603−6604.

(14) Nishizawa, M.; Menon, V. P.; Martin, C. R. *Science* **1995**, *268*, 700−702.

(15) Hou, Z.; Abbot, N. L.; Stroeve, P. *Langmuir* **2000**, *16*, 2401−2404.

(16) Chun, K.-Y.; Stroeve, P. *Langmuir* **2001**, *17*, 5271−5275.

(17) Hille, B. *Ionic Channels of Excitable Membranes*; Sinauer: Sunderland, 1992.
(18) Lev, A. A.; Korchev, Y. E.; Rostovtseva, T. K.; Bashford, C. L.; Edmonds, D. T.; Pasternak, CA. *Proc. R. Soc. London* **1993**, *252*, 187−192.
(19) Rostovtseva, T. K.; Bashford, C. L.; Alder, G. M.; Hill, G. N.; McGiffert, C. M.; Appel, P. Y.; Lowe, G.; Pasternak, CA. *J. Membr. Biol.* **1996**, *151*, 29−43.
(20) Siwy, Z.; Gu, Y.; Spohr, H. A.; Baur, D.; Wolf-Reber, A.; Spohr, R.; Apel, P.; Korchev, Y. E. *Europhys. Lett.* **2002**, *60*, 349−355.
(21) Siwy, Z.; Fulinski, A. *Phys. Rev. Lett.* **2002**, *89*, 198103−1.
(22) Siwy, Z.; Dobrev, D.; Neumann, R.; Trautmann, C.; Voss, K. *Appl. Phys. A* **2003**, *76*, 781−785.
(23) Apel, P.; Korchev, Y. E.; Siwy, Z.; Spohr, R.; Yoshida M. *Nucl. Instr. Methods Phys. Res. B.* **2001**, *184*, 337−346.
(24) Ramírez, P.; Mafé, S.; Alcaraz, A.; Aguilella, V. M. *Phys. Rev. E* **2003**, *68*, 011910−1.
(25) Ramírez, P.; Mafé, S. Ion equilibrium and transport in weak amphoteric membranes. In *Surface Chemistry and Electrochemistry of Membranes*; Sørensen, T. S., Ed.; *Surfactant Science Series*, Vol. 79; Marcel Dekker: New York, 1999; pp 437−454.
(26) Kontturi, K.; Mafé, S.; Manzanares, J. A.; Svarfvar, B. L.; Viinikka, P. *Macromolecules* **1996**, *29*, 5740−5746.
(27) Jimbo, T.; Higa, M.; Minoura, N.; Tanioka, A. *Macromolecules* **1998**, *31*, 1277−1284.
(28) Jimbo, T.; Tanioka, A.; Minoura, N. *J. Colloid Interface Sci.* **1998**, *204*, 336−341.
(29) Jimbo, T.; Tanioka, A.; Minoura, N. *Langmuir* **1998**, *14*, 7112−7118.
(30) Eisenberg, R. S. *J. Membr. Biol.* **1996**, *150*, 1−25.
(31) Martin, C. R.; Nishizawa, M.; Jirage, K.; Kang, M. *J. Phys. Chem. B* **2001**, *105*, 1925−1934.
(32) Martin, C. R.; Nishizawa, M.; Jirage, K.; Kang, M. Lee, S. B. *Adv. Mater.* **2001**, *13*, 1351−1362.
(33) Buck, R. P. *J. Membr. Sci.* **1984**, *17*, 1−62.
(34) Pellicer, J.; Mafé, S.; Aguilella, V. M. *Ber. Bunsen-Ges. Phys. Chem.* **1986**, *90*, 867−872.
(35) Helfferich, F. *Ion Exchange*; McGraw-Hill: New York, 1962.
(36) Sørensen, T. S.; Rivera, S. R. Electrochemical Characterization of Membranes and Membrane Surfaces by EMF Measurements. In *Surface Chemistry and Electrochemistry of Membranes*; Sørensen, T. S., Ed.; *Surfactant Science Series*, Vol. 79; Marcel Dekker: New York, 1999; pp 313−397.
(37) Ramírez, P.; Alcaraz, A.; Mafé, S.; Pellicer, J. *J. Colloid Interface Sci.* **2002**, *253*, 171−179.
(38) Manzanares, J. A.; Vergara, G.; Mafé, S.; Kontturi, K.; Viinikka, P. *J. Phys. Chem. B* **1998**, *102*, 1301−1307.
(39) Menon, V. P.; Martin, C. R. *Anal. Chem.* **1995**, *67*, 1920−1928.
(40) Chun, K.-Y.; Stroeve, P. *Langmuir* **2002**, *18*, 4653−4658.
(41) Yu, S.; Lee, S. B.; Kang, M.; Martin, C. R. *Nano Lett.* **2001**, *1*, 495−498.
(42) Kang, M.; Martin, C. R. *Langmuir* **2001**, *17*, 2753−2759.
(43) Kang, M.; Martin, C. R. *Chem. Rev.* **2000**, *100*, 2575−2594.
(44) Jirage, K. B.; Hulteen, J. C.; Martin, C. R. *Science* **1997**, *278*, 655−658.
(45) Press: W. H.; Teukolsky, S. A.; Vetterling, W. T.; Flannery, B. P. *Numerical Recipes in Fortran 77: The art of Scientific Computing*; Cambridge University Press: New York, 1992.
(46) Ramírez, P.; Alcaraz, A.; Mafé, S.; Pellicer, J. *J. Membr. Sci.* **1997**, *135*, 135−144.
(47) Robinson, R. A.; Stokes, R. H. *Electrolyte Solutions*; Butterworth Scientific Publications: London, 1955.
(48) Mafé, S.; Manzanares, J. A.; Pellicer, J. *J. Membr. Sci.* **1990**, *51*, 161−168.
(49) Westermann-Clark, G. B.; Anderson, J. L. *J. Electrochem. Soc.* **1983**, *130*, 839−844.
(50) Kanicky, J. R.; Shah D. O. *J. Colloid. Interface Sci.* **2002**, *256*, 201−207.
(51) Saito, K.; Tanioka, A. *Polymer* **1996**, *37*, 2299−2302.
(52) Ramírez, P.; Mafé, S.; Tanioka, A.; Saito, K. *Polymer* **1997**, *38*, 4931−4934.